Electronic Supplementary Material (ESI) for New Journal of Chemistry.
This journal is © The Royal Society of Chemistry and the Centre National de la Recherche Scientifique 2023

Supporting Information

Electrochemical assembly of flexible PPy/Bi-Te alloy/PPy thermoelectric composite films with a sandwich-type structure

Yang Li,[ab†] Zhi-Ping Chen,[ab†] Cai-Yan Gao,*[a] Hui-Ping Li,[ab] Xin-Heng Fan,[a] Xingbo Cao[a] and Lian-Ming Yang*[a]

[a]*Beijing National Laboratory for Molecular Sciences (BNLMS), Key Laboratory of Green Printing, Institute of Chemistry, Chinese Academy of Sciences, Beijing 100190, P. R. China;* [b]*University of Chinese Academy of Sciences, Beijing 100049, P. R.* [†]*The authors contributed equally to this work. China.*

E-mail: gaocaiyan@iccas.ac.cn; yanglm@iccas.ac.cn

List of Contents

1. Materials S3
2. Electrochemical assembly of PPy/Bi-Te alloy/PPy composites..... S3
3. Measurements and characterizations..... S4
4. Calculation of grain size and crystal orientation..... S5
5. Assembly of the F-TEGs..... S6
6. Supplemented electrochemical measurements..... S6
7. SEM supplemented images..... S7
8. EDS supplemented data S8
9. HRTEM supplemented images S8
10. Raman spectroscopy S9
11. Comparison of thermoelectric (TE) and mechanical properties S10
12. Influence of the PPy on the TE performance of the Bi-Te alloy S11
13. Influence of the Bi-Te alloy on the doping levels of PPy S11
14. Schematic diagram of output performance measurement S11
15. References.....S11

1. Materials

All the chemical reagents were commercially available. Pyrrole (Py, 99 %), *p*-toluenesulfonic acid monohydrate (*p*-TSA, 99 %), bismuth(III) nitrate pentahydrate ($Bi(NO_3)_3 \cdot 5H_2O$, 99 %), ethylenediaminetetraacetic acid disodium salt (EDTA-2Na, 99 %), and sodium tellurite (Na_2TeO_3, 97 %) were purchased from Beijing Innochem Science & Technology Co., Ltd. Anhydrous ethanol (AR, ≥ 99.7 %), and acetone (AR, ≥99.5 %) was purchased from Tianjin Concord Technology Co., Ltd. Deionized water (Di-water) was prepared in laboratory. Py was purified by vacuum distillation. Other reagents were used as received without any further purification or treatment.

2. Electrochemical assembly of PPy/Bi-Te alloy/PPy composites

Three-electrode system and the pre-treatment of stainless-steel (SS) electrodes. In the three-electrode system, the platinum (Pt) sheet was used as the counter electrode (CE), the Ag/AgCl electrode as the reference electrode (RE), and the pretreated SS sheet as working electrode (WE). In a pretreatment process, a SS was firstly polished with 1500 mesh sandpaper in one direction and then put into acetone solution to undergo ultrasonic cleaning for 30 min, and finally a PVC tape was used to reserve an effective area of 4 cm^2 for PPy electrodeposition.

Electrodeposition of the underlying PPy layer. PPy layer was in-situ electrodeposited on SS electrode in an ice-water bath by galvanostatic method (GM). The precursor solution is an aqueous solution of Py (0.2 M) and *p*-TSA (1.0 M). The current density for Py electropolymerization was set as 1.0 mA cm^{-2}, and the deposition time was adjusted from 0 to 300 s. After the reaction was completed, the PPy film was washed with ethanol and Di-water for several times, and dried in vacuum at 70 ℃ for 6 h.

Electrodeposition of the Bi-Te alloy layer. The electrodeposition of Bi-Te alloy layer was carried out at room temperature. A SS coated by the PPy prepared as above

was used as the WE to deposit Bi-Te alloy layer in the precursor solution containing $Bi(NO_3)_3$ (8 mM), Na_2TeO_3 (10 mM), EDTA-2Na (8 mM), *p*-TSA (1.0 M), and the current density was constant at –0.8 mA cm^{-2}. The deposition time was controlled to 90 min to give the Bi-Te-base alloy layer with a constant thickness of about 1.8 μm. Finally, the same washing and drying procedures as described above were carried out.

Note: since the Bi-Te alloy layer directly electrodeposited on a SS is too brittle to be peeled off, an experimental manipulation reported previously[1] was adopted to solve this problem. That is, first depositing PPy pre-coating on a SS electrode, then depositing Bi-Te alloy layer, and finally peeling off the PPy bottom layer and Bi-Te alloy layer together by an insulating tape. A PPy layer is used as the pre-coating in this study to achieved a complete peeling of the Bi-Te alloy layer, further illustrating there is a very close contact between PPy and Bi-Te layers.

Electrodeposition of the top PPy layer. The upper PPy layer was deposited on the Bi-Te layer under the conditions consistent with those of deposition of the underlying PPy layer on SS layer. The composite film obtained was carefully peeled from the SS surface using a PVC tape for further tests and characterization.

3. Measurements and characterizations

The electrodeposition and cyclic voltammetry (CV) measurement were conducted using an electrochemical workstation (CHI660E, Chenhua Instruments Co., Shanghai, China). A voltage scan rate of 50 mV s^{-1} was used in cyclic voltammetry. Both electrodeposition and cyclic voltammetry studies were carried out at room temperature and in unstirred solutions. All CV curves were scanned first in the cathodic direction and the negative current density indicates a cathodic current. The Seebeck coefficient and the electrical conductivity were measured using a commercial Thin-Film Thermoelectric Parameter Test System (MRS-3RT, Wuhan Joule Yacht Science & Technology Co., Ltd, China) with a quasi-steady-state mode and a four-point configuration method, respectively. The morphologies of the composite films were observed by the field-emission scanning electron microscopy (FESEM, SU8020, HITACHI) equipped with an energy dispersive spectrometer (EDS, map-scanning mode) at an acceleration voltage of

5 kV. The high-resolution transmission electron microscopy (HRTEM, JEM-2100F, JEOL) was used to observe the internal nanostructures of PPy/Bi-Te/PPy composite. For HRTEM analysis, the samples were prepared using a focused ion beam (FIB, Helios NanoLab G3 CX, Thermo Fisher Scientific). During the FIB processing, a thin layer of Pt with thickness of around 0.4 μm was firstly deposited on the surface of the thin film to avoid ion damage. A cross-sectional lamella beneath the Pt layer was cut by high-energy Ga ion beams and was bonded to a post of copper lift-out grid with the FIB easy-lift system. The center area of the lamella was further thinned with low-energy Ga ion beams until the thickness was suitable for TEM observation. X-ray photoelectron spectroscopy (XPS) was performed on the Thermo Scientific ESCALab 250Xi (200 W monochromatic Al Kα radiation). The 500 μm X-ray spot was used for SAXPS analysis and the base pressure in the analysis chamber was about 3×10^{-9} mbar. Typically, the hydrocarbon C1s line at 284.5 eV from adventitious carbon is used for energy referencing. The Raman spectra of the samples were recorded by a Raman spectrometer (HORIBA LabRAM HR Evolution) with an excitation wavelength of 532 nm, and a Raman shift spectral range from 80 to 1880 cm^{-1}. Crystal structure of the films was examined by the X-ray diffraction (XRD) which was performed using an X-ray diffractometer (Rigaku, D/MAX RINT-2500) with Cu Kα radiation (λ = 1.54 Å) at a speed of 5° min^{-1}. The composite film was bent and fixed along a bar with a radius of 5 mm for a certain number of times to test its flexibility and electrical conductivity.

4. Calculation of grain size and crystal orientation

In order to further study the crystal growth of different composite films, the grain sizes and crystal orientation were calculated (**Fig. S15**). Crystal orientation is defined as the ratio of the intensity of the (003) XRD peak to the sum of the intensities of all peaks [∑(hkl)]. The grain sizes, D, are determined using the Debye–Scherrer's equation (3)[2]:

$$\boldsymbol{D = \frac{K\lambda}{B\cos\theta}} \quad (3)$$

where K is the constant 0.89, λ is the X-ray wavelength (1.54051 Å), B is the full-width half-maximum (FWHM, rad), and θ is the diffraction angle.

5. Assembly of the F-TEGs

The F-TEGs module consists of six strips (12.0 × 4.5 mm) of the optimal PPy/Bi-Te/PPy composite films which were stuck on a polyimide (PI) substrate with an interval of 2.5–3.0 mm and then were connected end to end using a sterling silver wire (diameter: 0.15 mm). Each strip was connected to the silver wire with a conductive silver pulp to reduce the contact resistance. After bonding, another layer of PI substrate was covered and cured for 12 h at 70 ℃ to obtain the final product F-TEG.

As shown in **Fig. S7**, the output performance of F-TEG was measured by using a simple self-made circuit. Its working process is as follows: when a fixed temperature difference ΔT is applied at both ends of the device, the output characteristics of the device are measured by adjusting the load resistance value R_L in the circuit. The parameters of the circuit are measured by a multimeter (VICTOR VC890D Pro).

6. Supplemented electrochemical measurements

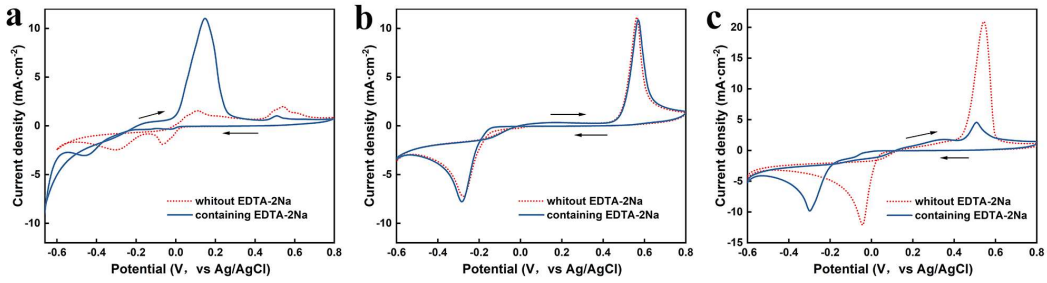

Fig. S1. Effect of EDTA-2Na on Bi (a), Te (b) and Bi-Te alloy (c) electrodeposition (SS as the WE; a scan rate of 50 mV s^{-1}) : (a) in the solid line, the electrolyte contains $Bi(NO_3)_3$ (8 mM), EDTA-2Na (8 mM) and *p*-TSA (1.0 M), and the electrolyte in the dashed line does not contain EDTA-2Na; (b) in the solid line, the electrolyte contains Na_2TeO_3 (10 mM), EDTA-2Na (8 mM) and *p*-TSA (1.0 M), and the electrolyte in the dashed line does not contain EDTA-2Na; and (c) in the solid line, the electrolyte contains $Bi(NO_3)_3$ (8 mM), Na_2TeO_3 (10 mM), EDTA-2Na (8 mM) and *p*-TSA (1.0 M), and the electrolyte in the dashed line does not contain EDTA-2Na.

7. SEM supplemented images

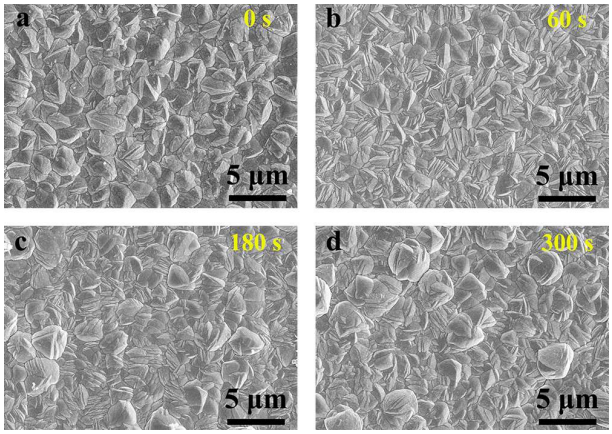

Fig. S2. SEM images of the surface morphology of Bi-Te alloy layer electrodeposited on the PPy layer with a deposition time of (a) 0 s; (b) 60 s; (c) 180 s; (d) 300 s.

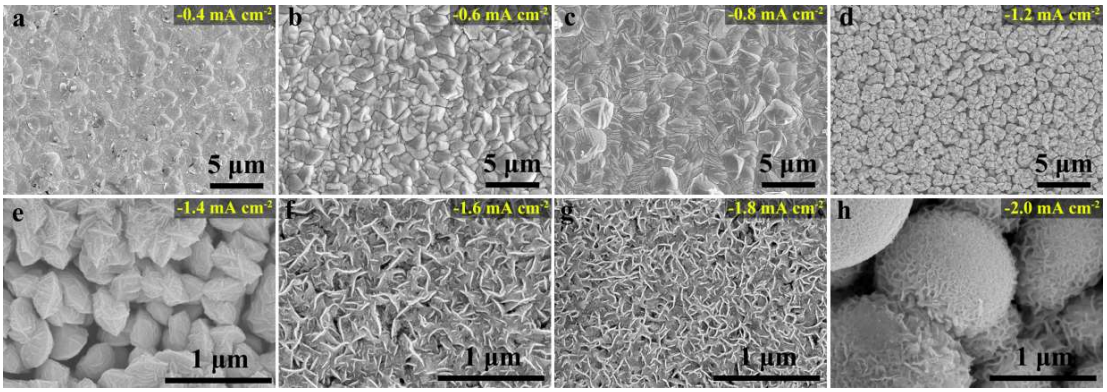

Fig. S3. The effects of the current density for the electrodeposition of Bi-Te alloy over the PPy layer on the SEM surface morphology of Bi-Te alloy.

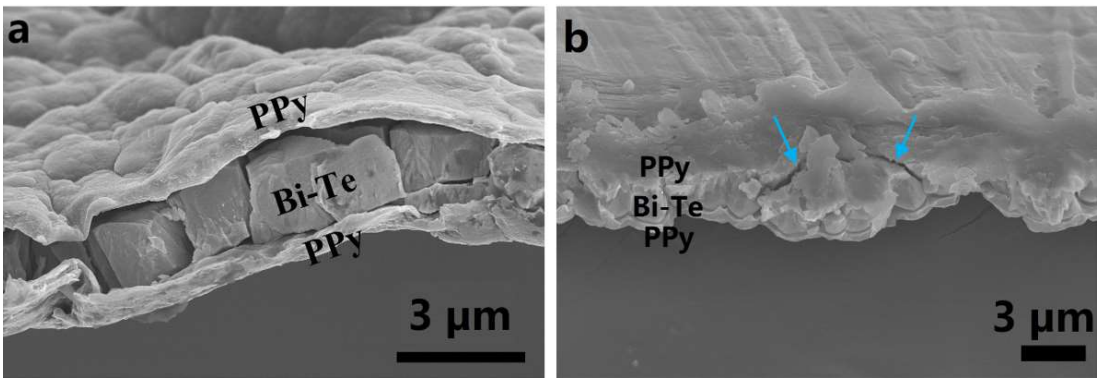

Fig. S4. (a,b) cross-sectional SEM images of the PPy/Bi-Te alloy/PPy composite film after being bent for 800 times (a) and 1000 times (b).

8. EDS supplemented data

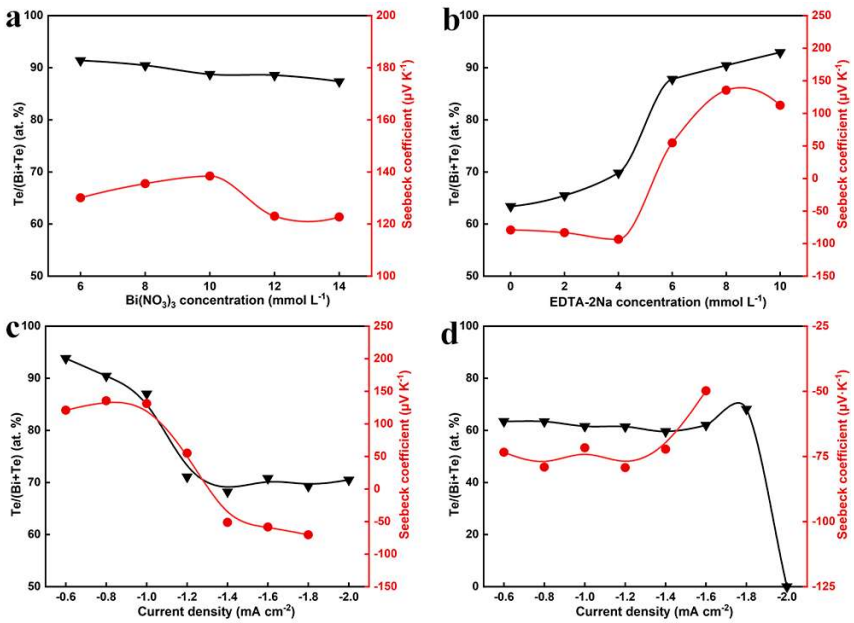

Fig. S5. Bi-Te alloy composition obtained from EDS measurement and Seebeck coefficient as a function of Bi-Te electrodeposition electrolyte concentration (the other electrolyte concentrations remain the same): (a) $Bi(NO_3)_3$ concentration (when it was $\geqslant$ 10 mmol L^{-1}, cracks appeared on the Bi-Te alloy layer); (b) EDTA-2Na concentration. Composition and Seebeck coefficient as a function of Bi-Te electrodeposition current density: (c) containing 8 mM EDTA-2Na; (d) not containing EDTA-2Na.

9. HRTEM supplemented images

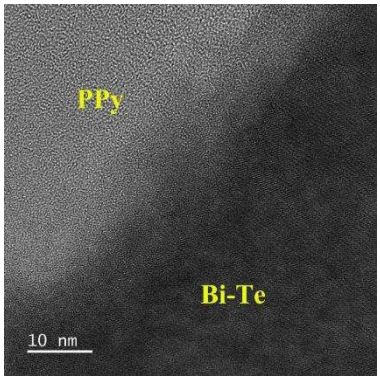

Fig. S6. HRTEM cross-section image of PPy and Bi-Te junction in the PPy/Bi-Te alloy/PPy composite film in **Fig. 5**a.

10. Raman spectroscopy

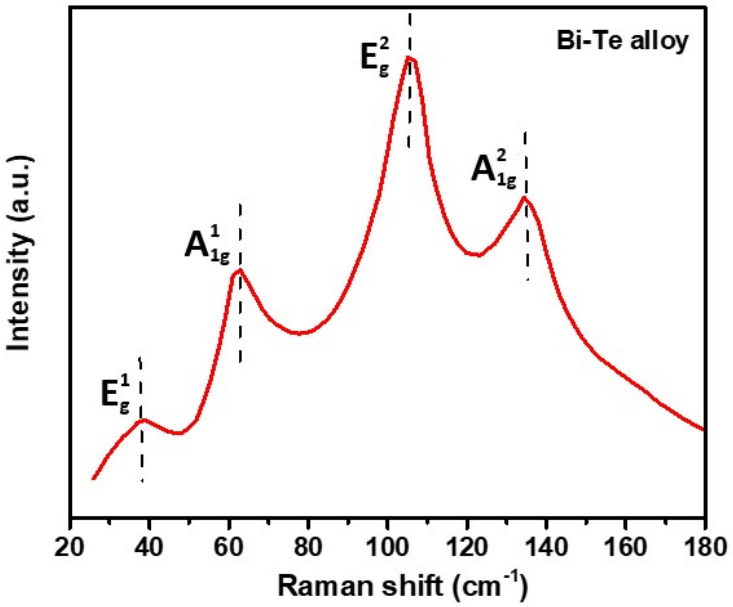

Fig. S7. Raman spectrum of the Bi-Te alloy layer.

11. Comparison of thermoelectric (TE) and mechanical properties

Table S1. A comparison of thermoelectric and mechanical properties of Bi-Te alloy/conducting polymer composite films at room temperature.

Composite	Preparation method	PF ($\mu W\ m^{-1}\ K^{-2}$)	ZT	Bending times (bending radius)	Retention rate of σ
Bi_2Te_3/PPy[3]	Spark plasma sintering, and then in-situ chemical polymerization	~2200 (n-type)	~0.98	–	–
Bi_2Te_3/PTh[4]	Spark plasma sintering	~110 (n-type)	~0.07	–	–
Bi_2Te_3/PTh[5]	Physical mixing, and then hot pressing	~1.8 (n-type)		–	–
Bi_2Te_3/P3HT[6]	Physical mixing, and then drop-casting	~13.6 (p-type)		–	–
Bi_2Te_3/PANI[7]	Hydro-thermal synthesis, and then in-situ polymerization	~1.5 (p-type)	~0.02	–	–
Bi_2Te_3/PANI[8]	Physical mixing, and then casting	~51 (p-type)	~0.18	–	–
Bi_2Te_3/PEDOT:PSS[9]	Two-step drop-casting	~70 (p-type), ~40 (n-type)		–	–
Bi_2Te_3/PEDOT:PSS[10]	Physical mixing, and then casting	~432 (n-type)	~0.18	1 (3.34 mm)	~98
Bi_2Te_3/PEDOT:PSS[11]	Melting, and and then in-situ polymerization	~3000 (n-type)	~0.8	–	–
Bi_2Te_3/PEDOT:PSS[12]	Physical mixing, and then drop-casting	~ 10.6 (p-type)	~0.01	–	–
Bi_2Te_3/PEDOT:PSS[13]	Physical mixing, and then drop-casting	~ 10 (p-type)	~0.04	–	–
PPy/Bi-Te alloy/PPy (this work)	Electrosynthesis	~274 (p-type)			

12. Influence of the PPy on the TE performance of the Bi-Te alloy

Table S2. A comparison of the TE performance for the different samples with or without the underlying PPy and/or the top PPy.

Sample	Electrical conductivity ($S\ cm^{-1}$)	Seebeck coefficient ($\mu V\ K^{-1}$)	Power factor ($\mu W\ m^{-1}\ K^{-2}$)
Pure Bi-Te alloy	30.4 ± 2.2	134.8 ± 4.68	55.9 ± 0.4
PPy/Bi-Te alloy[a]	112.1 ± 17.1	74.7 ± 1.9	62.2 ± 6.5
PPy/Bi-Te alloy/PPy[b]	460.6 ± 28.3	72.8 ± 2.1	243.7 ± 6.1

[a]The two-layered sample was obtained by depositing Bi-Te alloy on the underlying PPy that was deposited for 180 s; [b]The three-layered sample was obtained by depositing the top PPy for 180 s on the two-layered PPy/Bi-Te alloy sample.

13. Influence of the Bi-Te alloy on the doping levels of PPy

Table S3. Influence of the deposition of the Bi-Te alloy on the doping levels of the underlying and top PPy.

Sample[a]	S (atomic %)	N (atomic %)	[N]/[S] %
Pristine PPy	4.07	10.21	39.9
Underlying PPy (after depositing Bi-Te alloy)	1.86	6.91	26.9
Top PPy (deposited on PPy/Bi-Te alloy)	3.65	8.91	41.0

[a]The deposition time of PPy in all the samples is 180 s.

14. Schematic diagram of output performance measurement

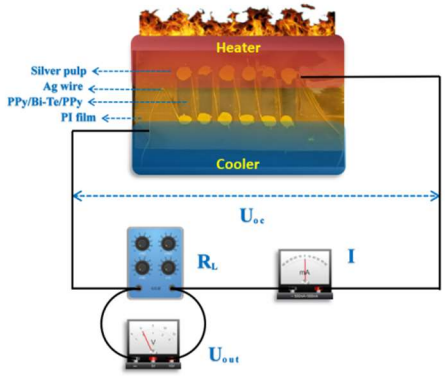

Fig. S8. A schematic diagram for the output performance measurement of the F-TEG.

15. References

[1] Y. Li, C.-Y. Gao, X.-H. Fan, L.-M. Yang, Full-electrochemical construction of high-performance polypyrrole/tellurium thermoelectrical nanocomposites, *ACS Appl.*

Mater. Interfaces **2022**, *14*, 10815–10824.

[2] B. Fang, Z. Zeng, X. Yan, Z. Hu, Effects of annealing on thermoelectric properties of Sb_2Te_3 thin films prepared by radio frequency magnetron sputtering, *J. Mater. Sci.* **2013**, *24*, 1105–1111.

[3] C. Kim, J. Y. Baek, D. H. Lopez, D. H. Kim, H. Kim, Interfacial energy band and phonon scattering effect in Bi_2Te_3-polypyrrole hybrid thermoelectric material, *Appl. Phys. Lett.* **2018**, *113*, 153901. https://doi.org/10.1063/1.5050089.

[4] W. Q. Ao, L. Wang, J. Q. Li, F. Pan, C. N. Wu, Synthesis and characterization of polythiophene/Bi_2Te_3 nanocomposite thermoelectric material, *J. Electron. Mater.* **2011**, *40*, 2027–2032. https://doi.org/10.1007/s11664-011-1664-3.

[5] Y. Du, K. F. Cai, S. Z. Shen, B. An, Z. Qin, P. S. Casey, Influence of sintering temperature on thermoelectric properties of Bi_2Te_3/polythiophene composite materials, *J. Mater. Sci.: Mater. Electron.* **2012**, *23*, 870–876. https://doi.org/10.1007/s10854-011-0509-4.

[6] M. He, J. Ge, Z. Lin, X. Feng, X. Wang, H. Lu, Y. Yang, F. Qiu, Thermopower enhancement in conducting polymer nanocomposites via carrier energy scattering at the organic–inorganic semiconductor interface, *Energy Environ. Sci.* **2012**, *5*, 8351–8358. https://doi.org/10.1039/C2EE21803H.

[7] K. Chatterjee, M. Mitra, K. Kargupta, S. Ganguly, D. Banerjee, Synthesis, characterization and enhanced thermoelectric performance of structurally ordered cable-like novel polyaniline–bismuth telluride nanocomposite, *Nanotechnology* **2013**, *24*, 215703. https://iopscience.iop.org/article/10.1088/0957-4484/24/21/215703.

[8] N. Toshima, M. Imai, S. Ichikawa, Organic–inorganic nanohybrids as novel thermoelectric materials: Hybrids of polyaniline and bismuth(III) telluride nanoparticles, *J. Electron. Mater.* **2011**, *40*, 898–902. https://doi.org/10.1007/s11664-010-1403-1.

[9] B. Zhang, J. Sun, H. E. Katz, F. Fang, R. L. Opila, Promising thermoelectric properties of commercial PEDOT:PSS materials and their Bi_2Te_3 powder composites, *ACS Appl. Mater. Interfaces* **2010**, *2*, 3170–3178. https://doi.org/10.1021/am100654p.

[10] G. Goo, G. Anoop, S. Unithrattil, W. S. Kim, H. J. Lee, H. B. Kim, M.-H. Jung, J. Park, H. C. Ko, J. Y. Jo, Proton-irradiation effects on the thermoelectric properties of flexible Bi_2Te_3/PEDOT:PSS composite films, *Adv. Electron. Mater.* **2019**,

1800786. https://doi.org/10.1002/aelm.201800786.

[11] C. Kim, J. Cho, T. Kim, D. H. Lopez, Interfacial effects in an inorganic/organic composite based on Bi_2Te_3 inducing decoupled transport properties and enhanced thermoelectric performance, *J. Mater. Chem. A* **2022**, *10*, 13780–13792. https://doi.org/10.1039/D2TA02334B.

[12] J. Xiong, L. Wang, J. Xu, C. Liu, W. Zhou, H. Shi, Q. Jiang, F. Jiang, Thermoelectric performance of PEDOT:PSS/Bi_2Te_3-nanowires: A comparison of hybrid types, *J. Mater. Sci.: Mater Electron* **2016**, *27*, 1769–1776. https://doi.org/10.1007/s10854-015-3952-9.

[13] Improved thermoelectric performance of free-standing PEDOT:PSS/Bi_2Te_3 films with low thermal conductivity, *J. Electron. Mater.* **2013**, *42*, 1269–1274. https://doi.org/10.1007/s11664-013-2587-y.